Chirality-mediated reentrant structure and dynamics in dense assemblies of active spinners

A Thesis

Submitted For the Degree of

Master of Science

by

Uttam Tiwari

CHEMISTRY AND PHYSICS OF MATERIALS UNIT,

JAWAHARLAL NEHRU CENTRE FOR ADVANCED SCIENTIFIC RESEARCH

Bangalore - 560 064

DECLARATION

I hereby declare that the matter embodied in the thesis entitled "**Chirality-mediated reentrant structure and dynamics in dense assemblies of active spinners**" is the result of investigations carried out by me at the Chemistry and Physics of Materials Unit, Jawaharlal Nehru Centre for Advanced Scientific Research, Bangalore, India under the supervision of Prof. Rajesh Ganapathy and that it has not been submitted elsewhere for the award of any degree or diploma.

In keeping with the general practice in reporting scientific observations, due acknowledgment has been made whenever the work described is based on the findings of other investigators.

Uttam Tiwari

CERTIFICATE

I hereby declare that the matter embodied in the thesis entitled "**Chirality-mediated reentrant structure and dynamics in dense assemblies of active spinners**" has been carried out by Mr. Uttam Tiwari at the Chemistry and Physics of Materials Unit, Jawaharlal Nehru Centre for Advanced Scientific Research, Bangalore, India under my supervision and that it has not been submitted elsewhere for the award of any degree or diploma.

Prof. Rajesh Ganapathy

Acknowledgment

First of all, I want to thank my supervisor, Prof. Rajesh Ganapathy, for his constant support, and guidance and for giving me the opportunity to work with him. This work would not have been possible without his valuable advice and support.

I am thankful to Prof. C.N.R Rao, FRS, for providing such excellent research facilities and environment at JNCASR. I would like to thank Prof. A. K. Sood for various scientific interactions. I am grateful to all the professors in JNC whose classes during the coursework greatly helped during my research work. I am very grateful to Pragya Arora, my senior in the lab, and my mentor, who helped me during my experiments and analysis of data with her valuable comments and advice.

I am very grateful to all my past and present members of the Soft and Active Matter Lab who helped me during my MS thesis, Monodeep, Niloyendu, Navneet, Pragya, and Kamlesh. I am grateful to my batchmates Aashish, Surabhi, Dipanjana, Sohini, Tarak, Arif, and Animesh for all the fun we had from day one in JNC. I thank all my friends in JNC who have made my journey in JNC memorable so far. Finally, I would like to acknowledge my mother and father who supported me throughout my life.

Synopsis

The emergence of collective behavior in active matter systems - assemblies of self-propelled particles - is by far the most exciting phenomenon in non-equilibrium statistical mechanics and condensed matter physics. In this thesis, we study dense assemblies of active rotors. By systematically changing the net chiralities of these systems, we enquire its role in the physics that emerges.

This thesis consists of three chapters. Chapter 1 provides a brief introduction to active matter and chiral active matter systems. Many experiments with striking emergent properties like odd viscosity, robust edge flow, oscillating edge current, and emergent stereoselective interactions and self-recognition have also been discussed. Chapter 2 discusses the experimental apparatus that has been designed to generate a well-controlled vertical vibration system. We then describe and explain the design of our chiral granular particles and how we exploit 3D printing to make them. Chapter3 discusses the

findings from our study. We report that dense assemblies of chiral rotors show a re-entrant in the structure, and we try to couple this re-entrant with the dynamics of the active rotors. We provide a qualitative argument about why such features can emerge in these systems. Also, in contrast to the Read and Shockley model, our experiment shows that the number of dislocations per unit length of grain boundary does not saturate with the increasing relative orientation of two grains.

List of Figures

Contents

Chapter 1

Introduction

The emergence of collective behavior in active matter systems - assemblies of self-propelled particles - is by far the most exciting phenomenon in non-equilibrium statistical mechanics and condensed matter physics. These collective behaviors include flocking of birds, schooling of fish (see Figure 1.1), and swarming of insects to name a few. The emergence of collective behavior becomes much more exciting with the introduction of chirality in active matter systems. An active system becomes chiral when there is a well-defined handedness in the particle's trajectory which can arise from an active torque on the particle. An active rotor [7], for example, has its legs designed in such a way that the particle gets an active torque and, depending on the way in which legs are tilted, the rotor will move either clockwise or anticlockwise thus, bringing chirality into its dynamics. Other examples include assemblies of spinning granules [13] and colloidal magnets [14]. Since many intriguing novel emergent behaviors come about in chiral active matter systems, there has been an increasing interest in studying them. Odd viscosity [6], odd diffusivity [15], stereoselective interactions and self-recognition [9], oscillating collective edge flow [8], etc., are a few examples of emergent properties in chiral active matter systems.

Most of the studies so far in chiral active matter have focussed on enantiopure systems (i.e., net chirality, $\chi = 1$). The question addressed in this thesis is how emergent properties

change and what new features arise when the net chirality in the system is systematically varied.

Figure 1.1: Polar order in a fish school. Figure from Jon Bertsch, from underwater images from the Sea of Cortez: http://www.thalassagraphics.com/blog/? p=167.

1.1 Active matter

Active matter comprises particles that use the energy available to them to convert it into motion [11] and the direction of motion is decided by the particles themselves rather than any external field. The energy input in the case of active matter is local, i.e., this energy input is at each particle level which is different from other non-equilibrium processes where the energy input is at the boundary of the system as in the case of shear flow. Thus, active matter systems break time-reversal symmetry and this takes these systems away from the equilibrium, resulting in their many novel properties, which include motility-induced phase separation [16], self-jamming, giant number fluctuations [2, 17], unexpected rheological and mechanical properties like the solid-like behavior of contractile active fluids in an orientationally ordered state show solid-like behavior [18] and also, the existence of a yield shear[19].

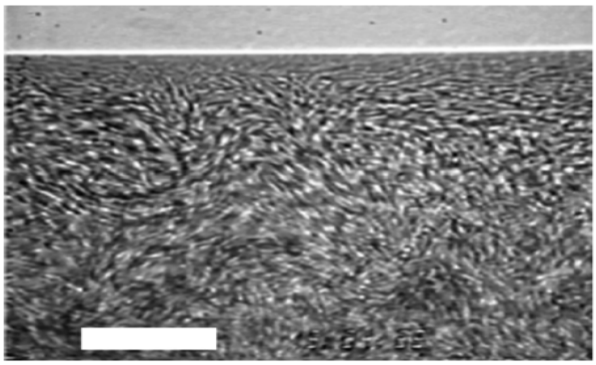

Figure 1.2: Bacterial "turbulence" in a sessile drop of Bacillus subtilis. Adopted from [1].

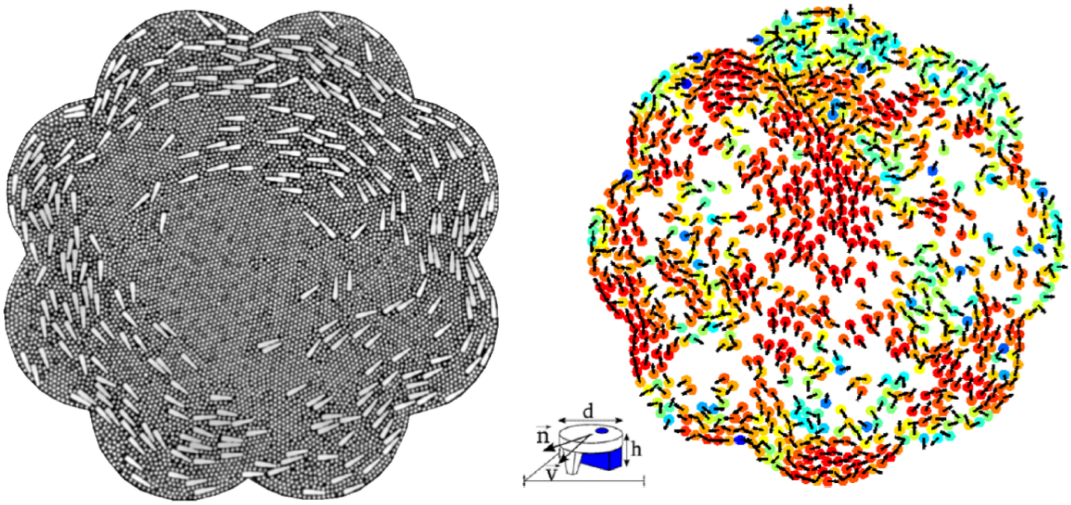

(a) (b)

Figure 1.3: A granular flock, a) millimetre-sized tapered brass rods align spontaneously on a vibrating surface. Adopted from[2], (b) Collective motion of self-propelled disks. Adopted from[3]

All-natural and inanimate systems which can self-propel come under the umbrella of active matter. Examples of the living system include bacterial suspensions (see Fig. 2), cell layers (see Fig. 3a), etc., while vibrated granular rods (see Fig. 3b), vibrated polar disks, self-propelled colloidal particles[20], come under the category of inanimate systems.

1.1.1 Simple models to describe flocks, herds, and schools

Craig W. Reynolds 1987 made the first attempt to understand large-scale coherent motion through a computer simulation [21]. He showed that one could get coherent motion by following some simple set of rules. These rules are stated below.

- No collision with the neighboring flockmates
- Align the velocity parallel to the neighboring flockmates.
- Remain close to the neighboring flockmates.

The other model which describes the emergent coherent motion is the Vicsek Model [22]. According to this model, any given particle, driven constantly with some velocity, rotates its direction of velocity at every time step and aligns it parallel to the average of its neighbours' velocities.

The above two models are the most basic ones for active matter and indeed we see coherent motion for both the models as the system's number density is increased or the strength of noise is decreased. The system remains disordered and isotropic at low density and large noise.

The above-mentioned models have certain limitations, for example, these models do not consider the polarity of the particle in explaining the interaction also, they do not talk about the medium (fluid) in which the particles are moving to explain the interactions. Thus, while these models are not well-suited to explain wet active matter systems, like assemblies of motile bacteria or fish schools, they are the building blocks for dry active matter systems.

1.1.2 Characterization of active matter: mean square displacement (MSD) and effective temperature

The simplest readout of active matter dynamics is the single-particle mean square displacement (MSD). MSD provides information on how much a particle displaces from its position at time t = 0.

Mathematically MSD is defined as;

$$\text{MSD} \equiv \langle |x(t) - x_0|^2 \rangle = \frac{1}{N} \sum_{i=1}^{N} |x^{(i)}(t) - x^{(i)}(0)|^2$$

MSD in experiments can be calculated from particle trajectory, which we obtain from imaging particle dynamics and then tracking their position through particle tracking algorithm. MSD for passive particle in two-dimension is given by Ornstein-Uhlenbeck formula [23], in two dimensions it reads as, $MSD(\tau) = 4D_T\tau + \frac{4k_BT}{m}\tau_m^2[e^{-\tau/\tau_m} - 1]$, which at longer time scales reduces to $MSD(\tau) = 4D_T\tau$. Here, D_T is the diffusion coefficient of particle and τ is time. For the case of active particles MSD reads as, $MSD(\tau) = [4D_T + 2v^2\tau_R]\tau + 2v^2\tau_R^2[e^{-\tau/\tau_R} - 1]$. Here, v is the velocity of self-propulsion, D_T is the diffusion coefficient of the particle. For active particles at short time scales, MSD(τ) $\propto$ τ, at intermediate time scales MSD(τ) $\propto \tau^2$, at long time scales again MSD(τ) $\propto \tau$ (see Figure 1.4).

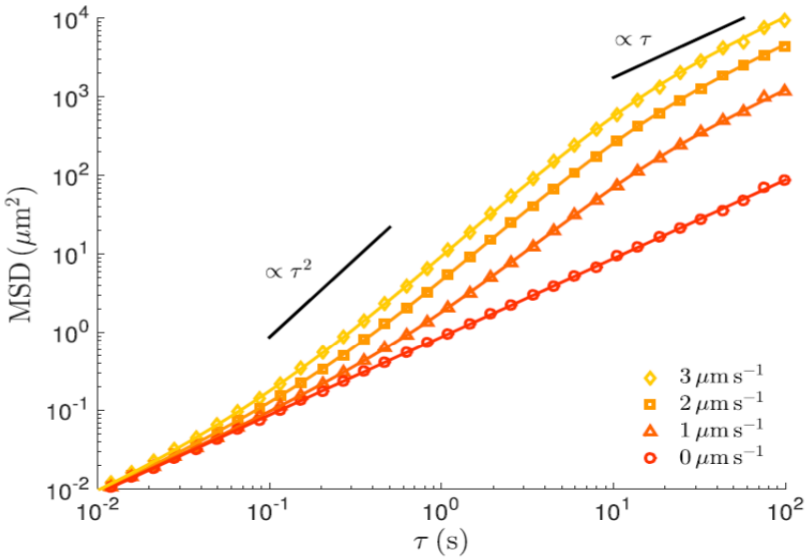

Figure 1.4: Mean square displacement (MSD) of active Brownian particles. For a passive particle [MSD(τ) $\propto \tau$], for active particle at short time scales [MSD(τ) $\propto \tau$], at intermediate time scales [MSD(τ) $\propto \tau^2$], at long time scales again [MSD(τ) $\propto \tau$]. Adopted from [4]

1.1.3 Classification of active matter systems

This section summarizes how the dynamics of an active particle change with time. To get an idea about the role of particles' polarity and the fluid in which these active particles are suspended, we next look at the different classifications of active matter systems.

Active matter systems can be classified as scalar or polar or nematic based on the order parameter used to classify them. Scalar active matter systems lack alignment interactions and the number density is the relevant order parameter. Examples of scalar active matter systems include, vertically vibrated granular disks and self-propelled colloidal spheres.

When active particles further possess alignment interactions, they can be further classified as polar or nematic

1. **Polar active particles**

   Elongated self-propelled polar objects, having distinct head and tail, order cooperatively either in the polar phase or nematic phase. When each active particle, on an

average, is aligned in the same direction, then we get a polar phase (see Figure 1.5). Bird flocks, bacteria swarms and fish schools are examples of polar-ordered phase.

2. **Active nematics**

We can get nematic ordering in two ways.

(a) When self-propelled polar objects in a system are parallel but there is a random head-tail orientation.

(b) When self-propelled particles are themselves symmetric with no distinction between head and tail.

An example of an active nematic includes microtubule bundles with ATP-powered kinase motor proteins binding them [24].

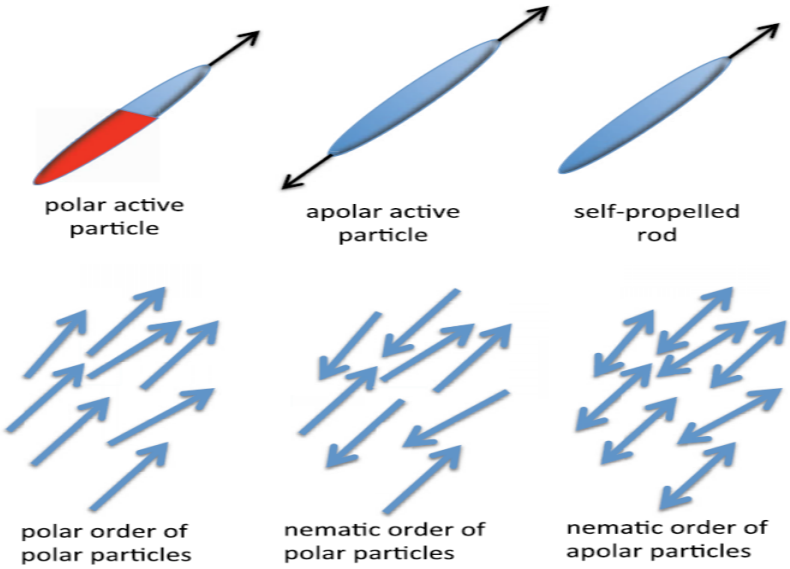

Figure 1.5: Schematic of the different of active particles and orientationally ordered states. Adopted from [5]

1.1.4 Classification of active matter based on the type of momentum damping: dry and wet systems

For some cases, one needs to consider the interaction between the particle and the fluid, in which the particle is suspended, to describe the physics of emergent coherent motion. This kind of system, where the fluid flow is vital to conserve momentum, is called a **'wet'** system. In this thesis, we will focus on dry active matter systems where the intervening fluid is absent and we will briefly discuss these systems below.

1.1.5 Dry Active Matter

An active system is 'dry' when there is no conservation of momentum. Vertically vibrated granular particles on a plate, animal herds on land are some examples of dry active matter. There is a loss of momentum in all the above-mentioned systems because of the friction between individual particles and the substrate. In the case of vertically vibrated granular particles, a substrate is a plate on which these particles move. If we neglect division and death, the conserved quantity for the dry active matter system is the total number of particles on the substrate. The focus of our thesis is *dry* chiral active matter system wherein we tune the net chirality to study different emergent properties in them. here, we first discuss some findings from achiral systems, and we then move to chiral systems.

Granules that are rendered active by vertical agitation have proven to be versatile model systems for probing the physics of dry active matter in the laboratory. Numerous studies have exploited the ease with which the shape of granules can be controlled to realize scalar, nematic, and polar active systems. While particles with isotropic and elongated shapes, under vertical agitation behave like scalar and nematic active systems [25], respectively, in order to achive polar active motion one usually tries to bring asymmetry by altering the shape of the particle. A particle with an asymmetric shape or with an asymmetric friction coefficient shows self-propulsion when vibrated vertically [11]. In

the study done by Julien Deseigne *et. al.* [3] a long-range collective motion was observed when disks having a built-in polar asymmetry in the friction coefficient were set to vibrate vertically between two horizontal plates (see Fig. 1.3b).

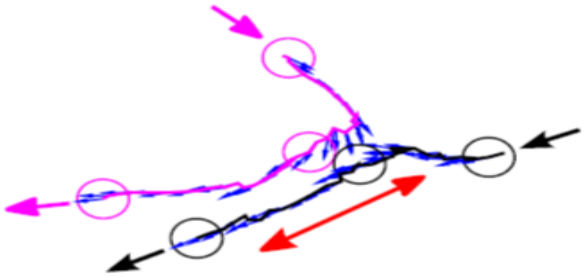

Figure 1.6: a) Trajectories shows how alignment occurs after the collision in vibrated polar disks b). Adopted from[3]

Polar alignment was seen after the collision between two particles (see Fig. 1.6). The collision between two particles, initially, shown in Fig. 1.6, was head-on but they get aligned after repeated contact with each other just after the initial collision.

Polar active motion has also been achieved in a system of millimeter-sized tapered rods [2]. Due to the tapering of the rods, these particles possess a fore-aft asymmetry in shape, which under vertical agitation renders them polar active.

While the studies above are by no means exhaustive, we refer the reader to the excellent review sriram2 where other example systems are described in detail.

1.2 Chiral Active matter

Both the time-reversal symmetry and the parity are broken in the case of chiral active fluids. The time-reversal symmetry breaking in the chiral active matter system gives rise to topological properties like one found in topological insulators and quantum Hall fluids. This includes the emergence of odd viscosity into a system of self-spinning particles. Stereoselective interactions and self-recognition, oscillating collective edge flow, etc. are

a few other examples of emergent properties in chiral active matter systems. We will discuss a few of the important emergent properties of chiral active matter in some detail.

1.2.1 Odd Viscosity

The fluid's viscosity is characterized by the resistance it offers to the applied shear rate. The odd viscosity of a fluid, on the other hand, is characterized by the various anomalous properties that arise in the chiral active fluid. For example, the flow is generally parallel to the direction of the applied pressure for all achiral fluid while in the case of chiral fluid, because of the odd viscosity in chiral active matter, we get the flow that is perpendicular to the applied pressure. There is no energy dissipation because of odd viscosity.

Mathematically, viscosity is represented by η_{ijkl}, where η_{ijkl} is a tensor. This η_{ijkl} is the coefficient of proportionality between viscous stress and strain rate. Onsager reciprocity relation tells that if you have time-reversal symmetry in the system then η_{ijkl} should be symmetric under the exchange of first and last pairs of indices i.e. $\eta_{ijkl} = \eta_{klij}$. In a recent study, it has been shown that in the case of chiral active systems, where both parity and time-reversal symmetry is broken, one gets a dissipationless linear-response coefficient in the constitutive relation which is termed as odd viscosity or hall viscosity[6]. Mathematically odd viscosity is denoted by η^o_{ijkl} and this is anti-symmetric under the exchange of first and last pairs of indices i.e. $\eta^o_{ijkl} = -\eta^o_{klij}$. To understand the transverse flow in chiral systems, we next discuss the collision mechanism between two chiral active rotors having the same handedness.

We know that Burgers shocks in achiral fluids move in the direction parallel to the compression. In the case of chiral active fluids, with odd viscosity, the shock has an extra flow that is perpendicular to the direction of shock propagation. Figure 1.6 shows how one gets transverse flow in the case of chiral active fluids.

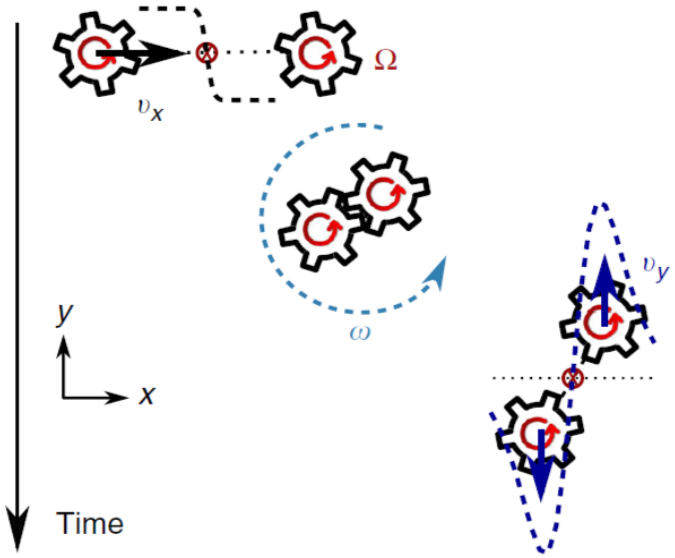

Figure 1.7: Schematic for the shock profile showing two self-spinning particles at different stages i.e., before, during, and after the collision. Adapted from [6]

A shock is propagating in the x-direction with speed v_x and this particle on the left side collides with the particle on right. As both the particles have intrinsic rotation Ω with them, during collision this intrinsic rotation is transformed into orbital rotation ω. As a result of the orbital rotation ω, after the collision, we also get the transverse flow. v_y is the amplitude of this transverse flow.

1.2.2 Boundary Flow

When the chiral active particle is made to vibrate in the confinement, a unidirectional flow along the boundary emerges. The direction of this flow depends on the chirality of the particle itself. The strength of this flow, apart from driving force, depends strongly on the curvature of the boundary and the particle density in the confinement[7]. In the recent study done by Xiang Yang *et. al.* it has been shown that this unidirectional flow is stronger when the shape of the boundary is concave. They also showed that the flow strength has a peak around the density $\phi = 0.65$.

Figure 1.8 shows the experimental and numerical values of the velocities for circular

confinement. The first figure shows v_θ, which quantifies flow parallel to the boundary, as a function of distance from the center for different values of particle density, and the second figure shows local angular velocity as a function of distance from the center.

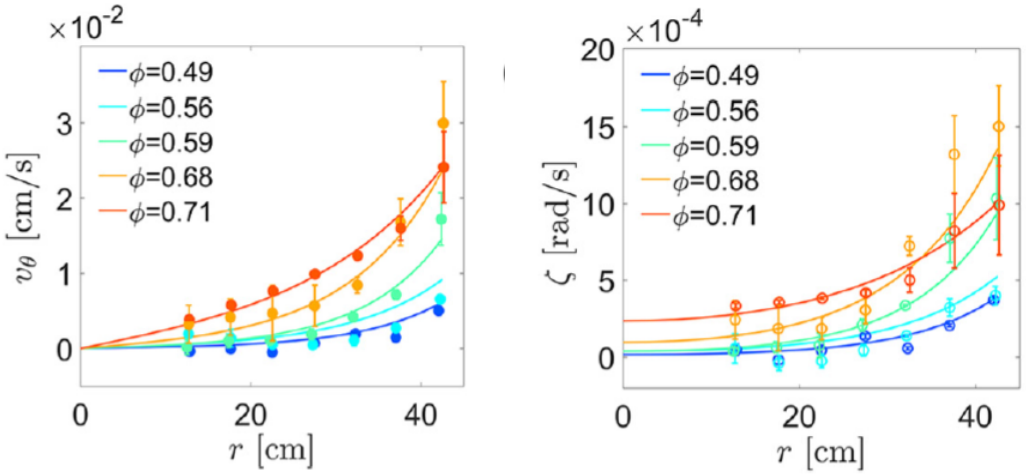

(a) (b)

Figure 1.8: Figure showing results in a circular confinement. (a) Radial profiles of $v_\theta(r)$, (b) Radial profiles of $\zeta(r)$. symbols represent experimental results and lines numerical represent results. Adopted from [7]

Indeed, we see that v_θ increases with an increase in the radial distance. The value of v_θ is maximum near the boundary for the value of density $\phi = 0.68$. The maximum value of v_θ is obtained for the maximum value of radial distance, indicating that edge flow is maximum or stronger near the confinement wall.

1.2.3 Oscillating collective motion

Oscillating collective motion is another type of collective behaviour shown by chiral active matter under confinement. The boundary wall for the passive system stops the particle from escaping and also brings in the surface tension. For the active case, the boundary wall leads to the emergence of oscillating collective motion which is absent in the case of passive systems. It has already been shown that there is the emergence of edge flow parallel to the boundary in the case of active rotors. Also for active rotors, as we saw

in the previous section, the intrinsic rotation of particles transforms into orbital angular momentum when two of them collide. In the case of active systems in confinement, one thing that can not be avoided is density inhomogeneity. This density inhomogeneity leads to oscillating edge flow in the case of confined active rotors[8].

Figure 1.8 below shows experimental (Figure 1.8 A) and simulation (Figure 1.8 B) results for orbital angular velocity (blue curve) and how it changes as you move from the center to the edge in the circular confinement. The magenta curve shows particle number density and how it changes as a function of radial distance.

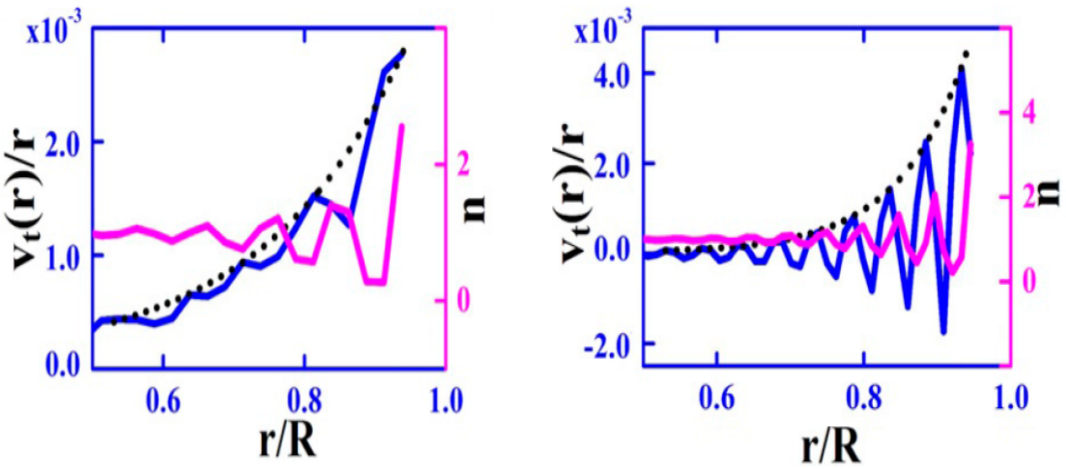

(a) (b)

Figure 1.9: The orbital angular velocity (blue) and the particle number density distribution (magenta) as a function of the radial distance. (a) Experimental results, (b) simulation results. The dashed lines are an exponential fit to the peak values of the orbital angular velocity. Adopted from[8]

There is a significant oscillation for orbital angular velocity and the amplitude of this oscillation decreases as the distance from the center decreases (see Figure 1.8), showing that edge flow is mostly present near the confinement wall.

1.2.4 Stereoselective Interactions and Self-recognition

The emergence of stereoselective interactions and self-recognition in a vertically vibrated monolayer of apolar chiral active ellipsoids is another unique emergent property in chiral active systems[9]. This study, done with 3D printed apolar chiral active ellipsoids, shows that when you have chirality encoded in just the dynamics of a particle, instead of chirality present as a static feature, one still gets stereoselective interactions and self-recognition. In the experiment with a racemic mixture, i.e., having the same numbers of particles with dextrogyre [(+)] and levogyre [(−)] trajectories, dimer formation was observed. A (+) and a (−) monomer having polar axis pointing in almost the same direction come together to form a "movers" state while in contrast, a (+) and a (−) monomer having polar axis pointing in the opposite direction come together to form "spinner" state (see Figure 1.7).

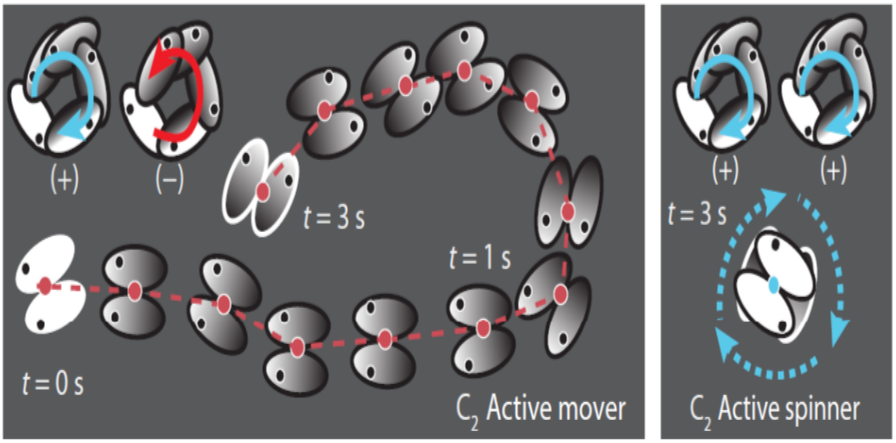

Figure 1.10: Stereoselective interactions in polar chiral active ellipsoids. (a) active mover, (b) active spinner. Adopted from [9]

1.2.5 Motivation for the present work

As is evident from the examples above, introducing chirality into active dynamics brings about enormous richness in dynamics. The bulk of the studies on chiral active systems has focused on assemblies where the chirality of all the particles have the same handedness. Furthermore, experiments on chiral active matter systems are few. With this in mind, in

this thesis, we develop a granular chiral active matter system, where the net chirality of the system can be varied from enantiopure to a racemic mixture. We will show that varying the net chirality quantitatively changes the structure and dynamics of dense assemblies of active spinners.

Chapter 2

Experimental Section

This chapter describes experimental techniques that were used to study the emergent properties in dense assemblies of chiral active disks. The first part of this section contains details about the experimental apparatus used to generate vertical vibration. The second part includes details on particle design and the mechanism of chiral active motion.

When it comes to vibrated granular matter experiments, the most crucial requirement is a well-controlled vibrational system. For the ideal case, one wishes to achieve vibration in only one degree of freedom with negligible lateral components. Electrodynamic shakers are most commonly used for creating such controlled vibration in granular matter experiments. These electrodynamic shakers are robust and can create the desired output but, due to internal resonances, they often bring in transverse motions. This non-axial motion, in our experimental apparatus, is taken care of by implementing an improved vibration system proposed by John Bush [10].

The chiral granular matter used for the experiment is fabricated using Multijet 3D printing. We will see in detail how this method allows us to print active rotors, used in the experiment.

2.1 Mechanical details of vibration system

Our apparatus provide precise verticle oscillation for the vertically agitated monolayer experiments (see Figure 2.1). This system provides controlled vertical sinusoidal acceleration with minimum lateral vibration. Following is detailed information about each component of the apparatus.

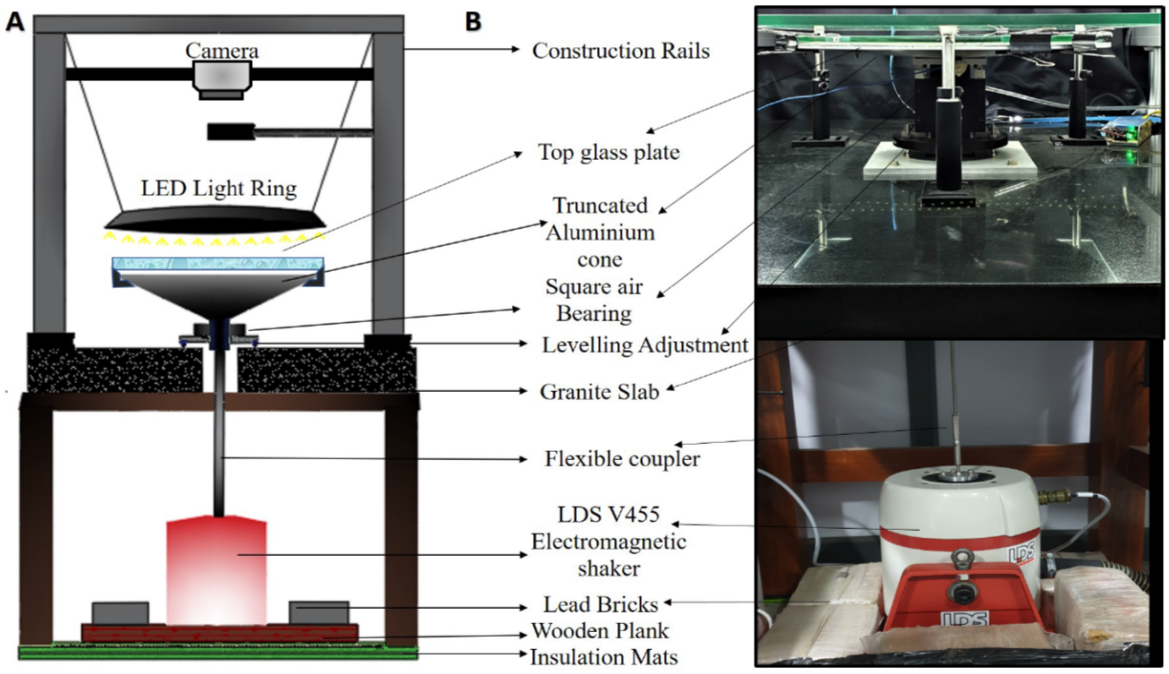

Figure 2.1: (A)schematic of the vertically vibrating apparatus. The diagram is not to scale.(B)Actual image of the setup

The electromagnetic shaker (LDS V455) provides the required sinusoidal vertical acceleration with a wide spectrum of frequency and acceleration values. A standard electrodynamic shaker, for the most extent, is similar to a loudspeaker. A coil of wire, suspended in a fixed radial magnetic fi

eld, drives the armature assembly(see Figure 2.2). A flexure plate provides mechanical support to the armature.

Lead bricks weighing 200 kg were placed on the wooden platform, with which the

shaker housing is bolted, to diminish the vibration of the support structure. Insulation mats, which separate the apparatus and the floor, decrease the transmission of vibration to the floor.

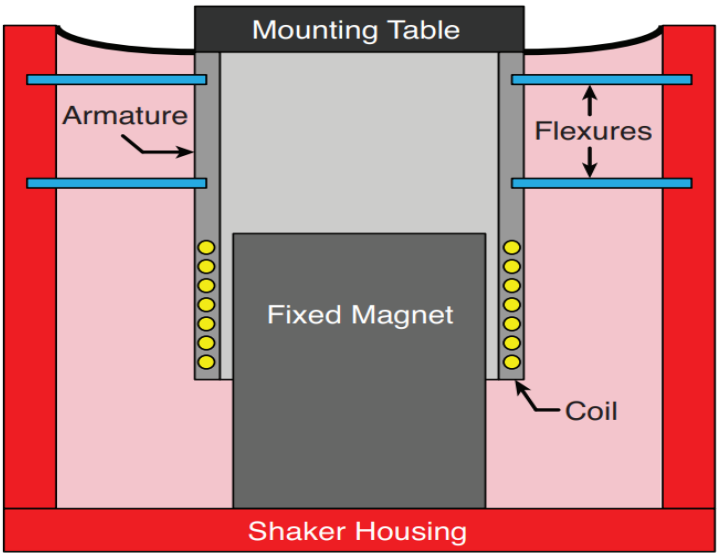

Figure 2.2: Schematic showing cross-section of a typical electrodynamic shaker. Adopted from [10].

A square-shaft low-friction air bearing (New Way Air Bearings) is used to transmit vibration from the shaker to the oscillating plate in the axial direction. This air bearing has a 75 mm slide for a 50mm X 50mm guide bar (see Figure 2.3). Submicron amplitude residual horizontal motion and virtually friction-free vertical oscillation are provided by the air bearing. Filtered air is supplied to the air bearing, and the pressure is maintained to 70 Psi.

The air-bearing carriage is connected to the leveling platform. The three locking screws in the platform are fixed to a circular breadboard. The air-bearing assembly is mounted on a table with a heavy granite top. A hole in the table allows the coupling of air bearing assembly to the electrodynamic shaker.

A thin drive rod made of stainless steel is used as a coupler to couple the guide bar to the shaker. The rod, 40 cm in length and 6 mm in diameter, connects the top of the

shaker to the bottom of the guide bar. The rod is flexible enough to take care of alignment mismatch.

A truncated aluminum cone, with a top diameter of 40 cm and a total height of 2 cm, acts as a substrate for granular particles and is attached to the top of the guide bar. Compared to the length scale of the roughness of the granular particles, the top of the truncated cone is machined to be perfectly flat.

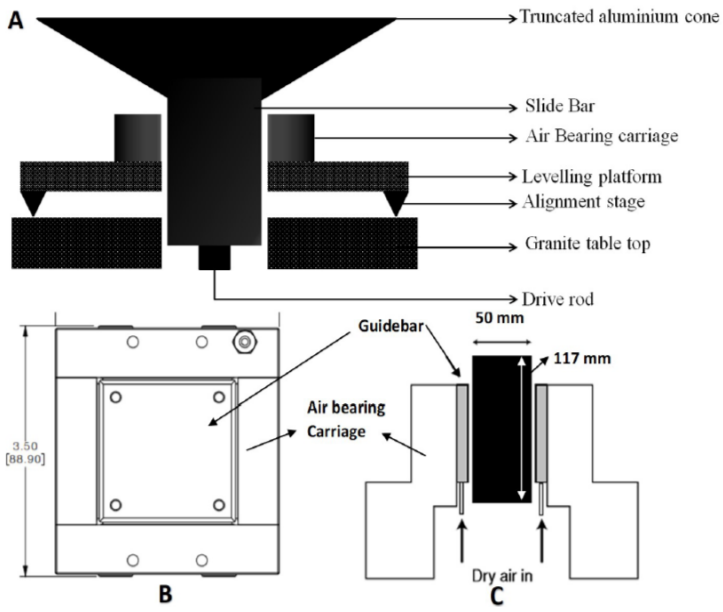

Figure 2.3: Schematic showing air bearing assembly.

The granular particles are confined between the aluminum plate and a circular glass plate. Glass plate on the top allows imaging for the particle on the substrate. The separation between the top and bottom plate is 2.4 mm, and the top plate is aligned with the bottom plate to maintain a uniform gap.

2.1.1 Control Electronics

A LDS LPA1000 power amplifier, connected to the LDS V455 shaker, is driven by Tektronix AFG 1062 function generator. Sinusoidal oscillation was generated using the function generator, and the experiment was done at a frequency value of 37 Hz.

2.2 Chiral active granular rotors

Self-propelled chiral particles were fabricated using Multijet 3D printing. We successfully designed clockwise and anticlockwise active rotors, having chirality encoded in the dynamics of particles, which were used to conduct experiments. This allowed us to characterize different emergent properties that arise due to the presence of chirality in the system.

2.2.1 Details of 3D printing

MultiJet Printing(MJP) uses piezo printhead technology to deposit either photocurable plastic resin or casting wax materials. MJP is used to build parts and molds with a high resolution to address a wide range of applications. Our 3D printer offers Z-direction resolution with a layer thickness of 16 microns. The particles were designed in *3D Builder* software, and the files containing the 3D design were fed to the printer in the stereolithographic(.stl) format.

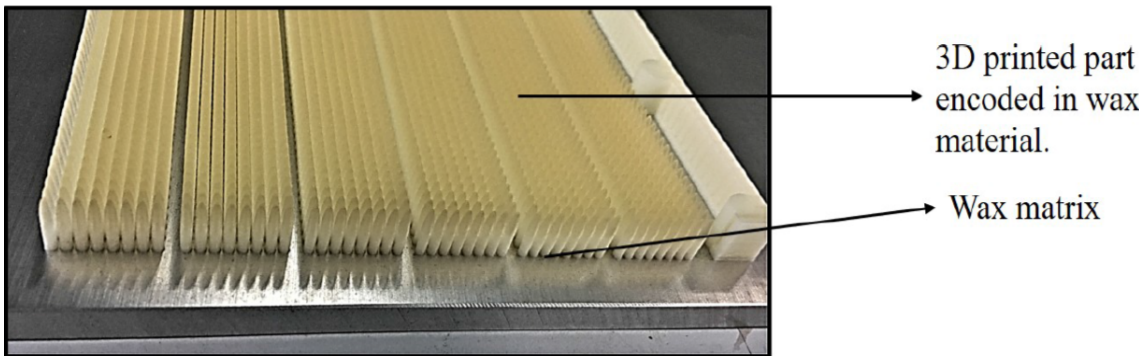

Figure 2.4: Batch of 3D printed particles.

Around 1200 particles were printed in one batch. Some parts of these particles were within wax molds that were cemented to the base of the tray. To get the particles out of the wax matrix, we sonicated them in oil at 60° Celsius, the temperature at which wax melts, and we are finally left with particles. These particles are then washed thoroughly with soap and water solution to remove oil from the surface. In the end, these particles

are washed with iso-propanol and are dried properly.

2.2.2 Mechanism of self-propulsion

A rod-shaped object tossed up in the vertically vibrated systems shows self-propulsion because of its shape, which breaks rotational symmetry. When such particles land, they are pushed away from the end which it first contacts the plate. The direction of propulsion is in the direction of the tilt of the rod(see Figure 1.5). The rod will be propelled towards one end if there is a difference in friction or weight between the two ends [5, 11].

The legs of chiral active particles are tilted rods arranged in a circular manner (see Figure 1.7), these legs together apply torque to the body of the chiral active particle, and depending on the direction of the tilt, we get either clockwise or anticlockwise rotors.

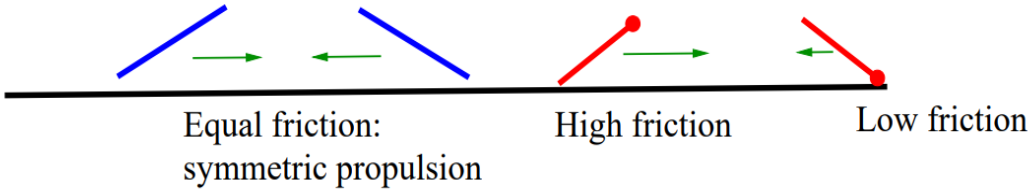

Figure 2.5: self propulsion of elongated rods. Adopted from [11]

2.2.3 Particles design

Our chiral active particle consists of two main parts: the dome-shaped body and inclined rod-shaped legs(see Figures 2.6 and 2.7). The dome is made by splitting an oblate ellipsoid. The splitting was made such that the plane of the split is perpendicular to the minor axis of the ellipsoid. The diameter of the circular base of the dome is 4.2 mm, and the total height of the dome is 1.05 mm. The legs are cylindrical in shape, having a base diameter of 0.35 mm. The legs are tilted at an angle of 25 degrees with the normal of the base of the dome.

Figure 2.6: Snapshots of chiral active particle.

There is a total of 16 legs in each of the chiral particles. The tilt direction decides whether the particle will be a clockwise rotor or an anticlockwise rotor when subject to vertical oscillation(see Figure 1.7). The total height of the particle, including the dome and the leg, is 1.8 mm. The direction of tilt of legs is the only parameter that differentiates between a clockwise and an anticlockwise rotor, and all other measurements remain the same. To differentiate between clockwise and anticlockwise rotors we have marked a circular dot on the clockwise rotor and a circle on the anticlockwise rotor. While a single tilted rod, as discussed earlier, shows self-propulsion in the direction of tilt, many such tilted legs attached to the periphery of any object will create an active torque.

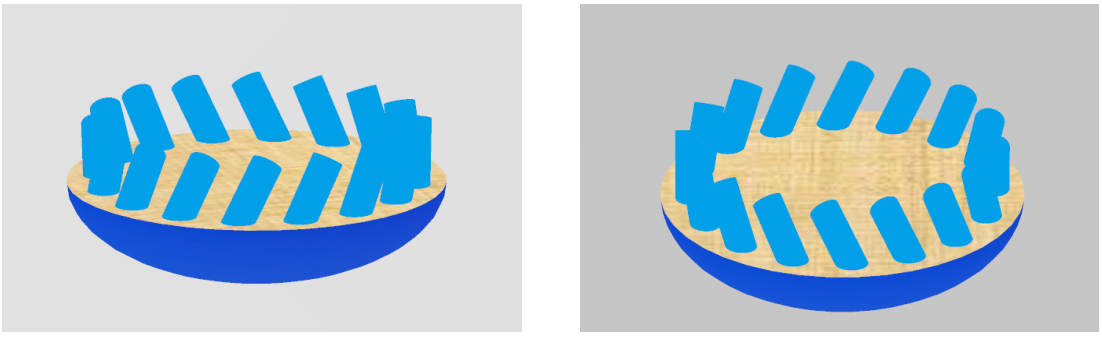

(a) (b)

Figure 2.7: Schematic showing chiral active particle (the particles are inverted to get a clear picture of design).(a) A anticlockwise rotor ,(b) A clockwise rotor.

2.2.4 Imaging and feature finding

A high-speed camera was used to image the particles. The frame rate, i.e., the number of frames per second was between 30 frames per second(fps) to 60 fps depending on the area fraction of the particles on the plate. The spatial resolution for the image was 2464 X 2056 pixels. Particles are lit uniformly with LED light surrounding the plate.

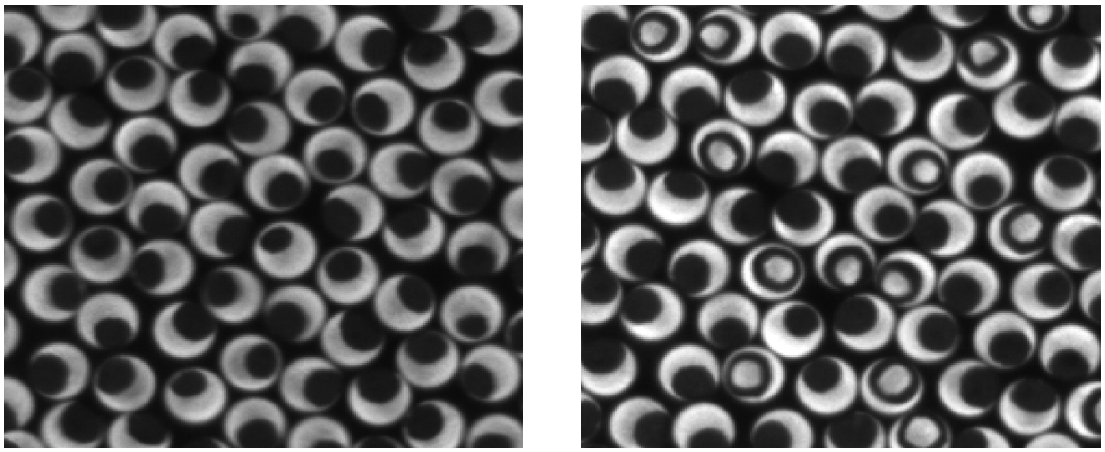

(a) (b)

Figure 2.8: Figure shows zoomed in view of chiral active particles on plate.(a) enantiopure, (b) racemic mixture of rotors.

MATLAB and ImageJ were used for image processing, and the centers of particles were obtained in MATLAB using standard algorithms. Fig 2.8 is the original image from the experimental data.

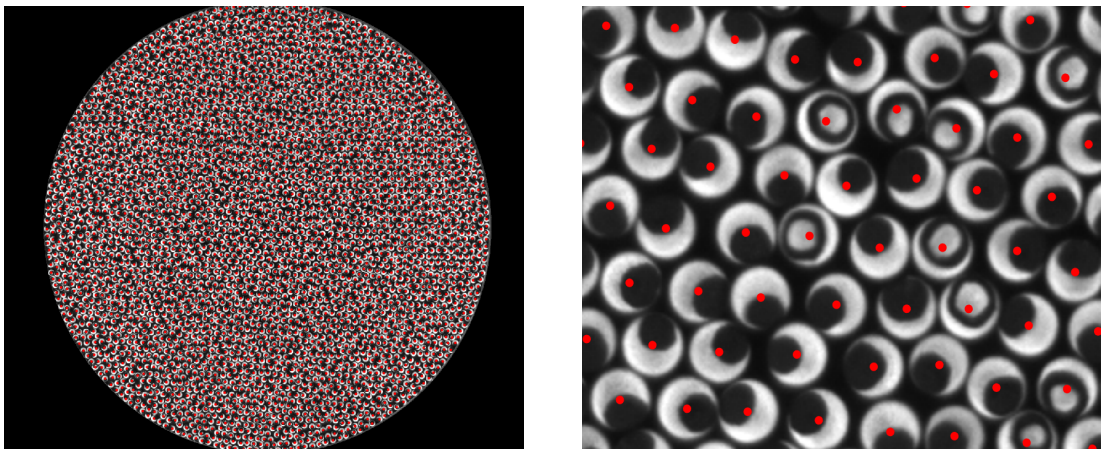

(a) (b)

Figure 2.9: Tracking of chiral active particle.(a) The red dots are the centres of particles, (b) Zoomed in view of figure a

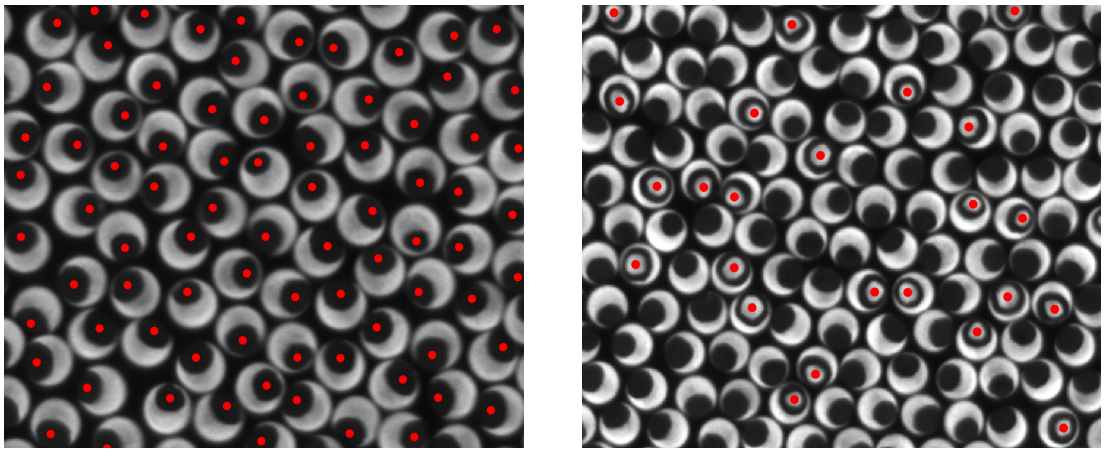

(a) (b)

Figure 2.10: Tracking of chiral active particle.(a) The red dots are the centres of blacks dot, marked on the clockwise rotors to get rotational information, (b) The red dots are the centres of circle, marked on the anticlockwise rotors to get rotational information.

Chapter 3

Results and discussion

This Chapter discusses findings from the experiment on dense assemblies of chiral active disks. First, we systematically varied the area fraction ϕ of the system, keeping the net chirality χ fixed, and then for a fixed value of ϕ, we varied the χ. Here, $\phi = \frac{N*a}{A}$, where N is the number of particles on the plate, a is the projected area of the individual rotor and, A is the area of the plate. The net chirality, χ, is defined as $\chi = \frac{|N_+ - N_-|}{N_+ + N_-}$, where N_+ and N_- are the fraction of monomers of clockwise rotors (+) and anticlockwise rotors (−), respectively. Since the rotors are essentially disks of uniform size, packing them at high densities resulted in packings that showed a high degree of crystallinity. Here we focus on ϕ's in the range $0.63 < \phi < 0.79$ while the net chirality for each of the ϕ's was varied from 0-1. All experiments were done for a fixed vibration frequency of 37 Hz. A key finding from these experiments is the observation of a reentrance in the number density of topological defects - dislocations on varying χ. By tracking the dynamics of individual rotors in both the rotational and translational degrees of freedom through their respective single-particle mean-squared displacements, we also attempt to provide a qualitative reasoning underlying this observation.

3.1 Observation of a re-entrance in the dislocation defect density with χ.

Our experimental system is comprised of clockwise and anticlockwise rotors within a circular boundary and confined between two horizontal plates.

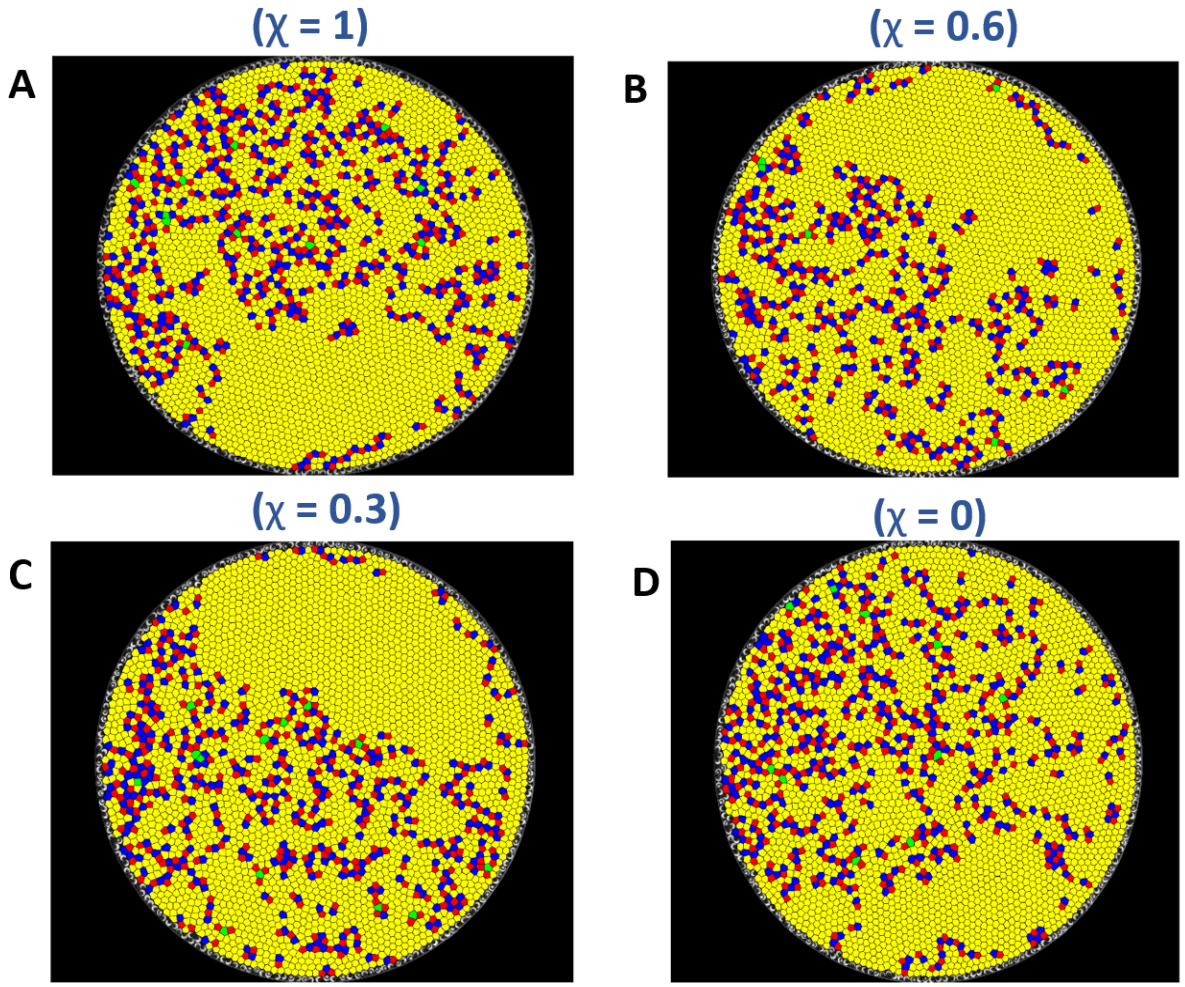

Figure 3.1: 5-7 pairs in the dense assemblies of active rotors at a fixed value of area fraction $\phi = 0.68$. (a) 5-7 pairs for $\chi = 1$, (b) 5-7 pairs for $\chi = 0.6$, (c) 5-7 pairs for $\chi = 0.3$, (d) 5-7 pairs for $\chi = 0$

To gain insights into the arrangement of the rotors in the circular confinement, we first performed a Voronoi tessellation for this system of circular rotors (see Fig. 3.1 for ϕ=0.68). The Voronoi tesselation is insensitive to the chirality of the individual disks and hence the

analysis provides information on the structural order of rotor packings. The Voronoi cells are color-coded according to the local coordination, while the yellow (hexagonal cells) color represents the particle with coordination number 6, the red (pentagonal cells), and blue (heptagonal cells) representing particles with a coordination of 5 and 7, respectively. We observed that defects in our system are almost entirely 5-7 pairs. Such a pair forms a topological defect with zero charge and is a dislocation. Isolated 5-, 7- coordinated particles were rare, and this is consistent with the expectation that such defects, which contribute to a non-zero local curvature, are energy expensive. Figure 3.1 shows how the total number of defects changes with the net chirality (χ).

In Fig. 3.2, we now plot the total number of defects for different ϕ as the net chirality is varied. To obtain statistically meaningful results, the Voronoi tessellation was done for over 14000 images for each ϕ and χ value.

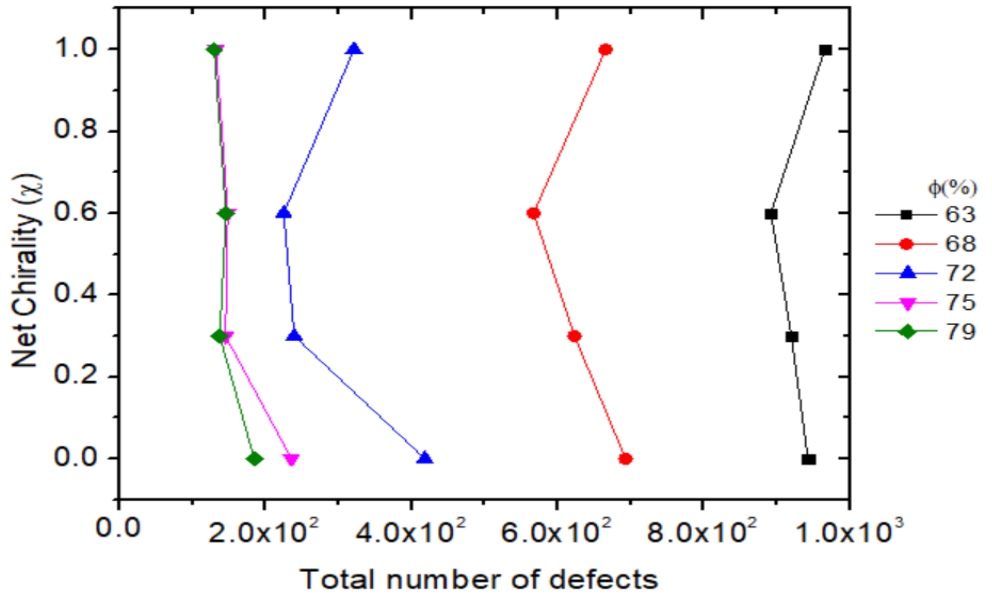

Figure 3.2: Reentrant behavior in the total number of defects on varying χ for various values of ϕ.

From Figure 3.2, it is evident that there is a clear re-entrant in the number of defects with net chirality, and for area fractions 0.68 and 0.72, this re-entrant is most significant, indicating an optimum density for observing such a behavior.

In the system of active rotors, having chirality encoded only in the dynamics of particles, the emergence of re-entrance opens up many questions. The first one is, does this re-entrant in the structure also manifest itself in the system's dynamics? We address this question by calculating the mean-squared displacement of the rotors in both the translational and rotational degrees of freedom.

3.1.1 Mean square displacement (MSD)

Mean square displacement (MSD), as already discussed in section 1.1.2, provides information on how much a particle displaces from its position at time t = 0, and thus can be best used in the quantification of dynamics.

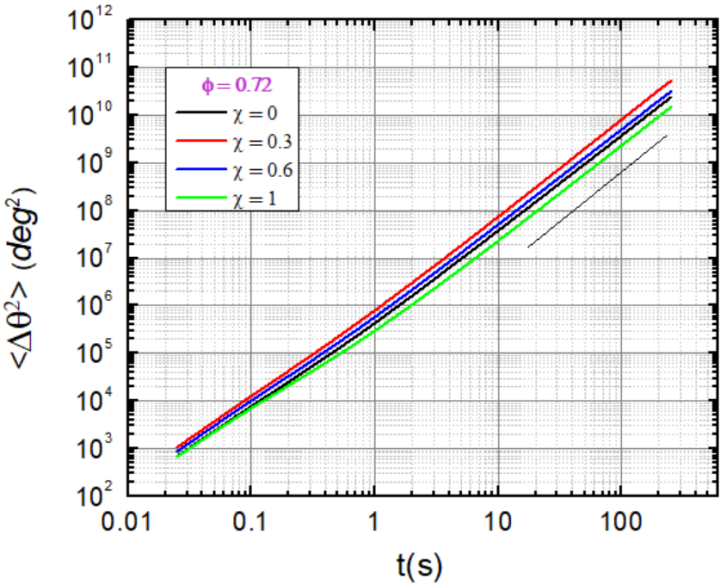

Figure 3.3: Angular mean square displacement (MSD) for the only clockwise rotors in a mixture of clockwise and anticlockwise rotors for different χ values at a fixed $\phi = 0.72$.

Figure 3.3 shows rotational MSD for only the clockwise spinners across different chiralities at the fixed value of area fraction $\phi = 0.72$. For t > 10s, the slope of these curves has a slope of ≈ 2, indicating that these chiral particles are rotationally superdiffusive for larger times, which is a characteristic of an active particle. Remarkably, the value of MSD

for $\chi = 0.3$ and $\chi = 0.6$ for any fixed t is always greater than the value corresponding to $\chi = 0$ and $\chi = 1$, indicating a clear re-entrant in the dynamics in the dense assemblies of active rotors. The key point to notice here is that for the intermediate values of chiralities, i.e., $\chi = 0.3$ and $\chi = 0.6$, which show faster dynamics, also contain fewer defects especially for $\phi = 0.68$ and $\phi = 0.72$. This observation uncovers a link between the reentrant behavior in structure and angular dynamics for active rotors.

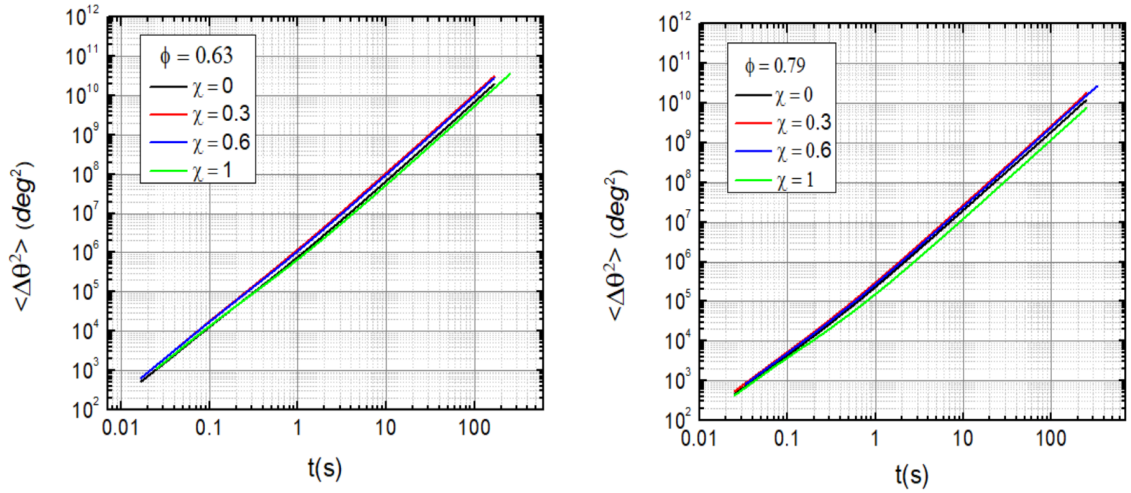

(a) (b)

Figure 3.4: Mean square displacement (MSD) for the clockwise rotors at diffrent chirality values. (a) MSD for $\phi = 0.63$, (b) MSD for $\phi = 0.79$.

To probe the re-entrant in dynamics at other area fractions, we plot the rotational MSD for $\phi = 0.63$ and $\phi = 0.79$ (see figure 3.4). The re-entrant is present for both the area fractions but the difference between MSD values among different chiralities is now reduced, showing that the strength of the reentrant behavior observed in the dynamics depends on ϕ. This was also the case with the number of defects, the maximum difference was found for $\phi = 0.68$ and $\phi = 0.72$, and this difference decreased for $\phi = 0.63$ and $\phi = 0.79$(see figure 3.2).

As a sanity check, we compared the dynamics of clockwise and anticlockwise rotors, which we expect to be identical. Figure 3.5 shows the MSD for both these rotors for

a racemic mixture ($\chi = 0$). Indeed, the MSD (figure 3.4), representing clockwise and anticlockwise rotors, almost completely overlap indicating that the dynamics of both rotors are identical within experimental uncertainty.

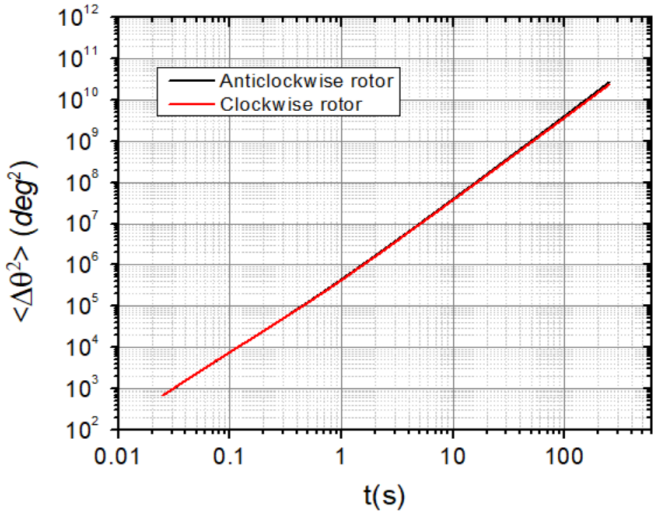

Figure 3.5: Rotational mean square displacement (MSD) for the clockwise and anticlockwise rotors at $\chi = 0$ and $\phi = 0.72$.

To gain further insight into the re-entrant dynamics, we plot the rotational MSD of clockwise and anticlockwise rotors in the dense assemblies of these chiral particles at area fraction $\phi = 0.72$ and, for $\chi = 0.3$ and $\chi = 0.6$. For $\chi = 0$ (figure 3.5), the difference between values of MSD, at a fixed t, for clockwise and anticlockwise rotors was negligible but with an increase in the net chirality, i.e., for $\chi = 0.3$ (see figure 3.6(a)), the difference became distinguishable and, for $\chi = 0.6$ this difference is much apparent (see figure 3.6(b)). We note here that as χ is increased from 0-1, the fraction of anticlockwise spinners in the system decreases systematically and is zero for $\chi = 1$ (enantiopure assembly of clockwise spinners).

The above observation suggests that the angular velocity of the anticlockwise rotor, the one which is fewer in number, is being boosted by the clockwise rotor due to a frictional coupling between them on contact. This analysis also reveals a plausible reason for the $\phi-$dependence observed in the reentrant dynamics (Fig. 3.2). For the boosting

of angular displacements by frictional coupling, the ϕ should be large enough for these rotors to frequently come in contact. But for very large ϕ, the system is more jammed and the dynamics slows down.

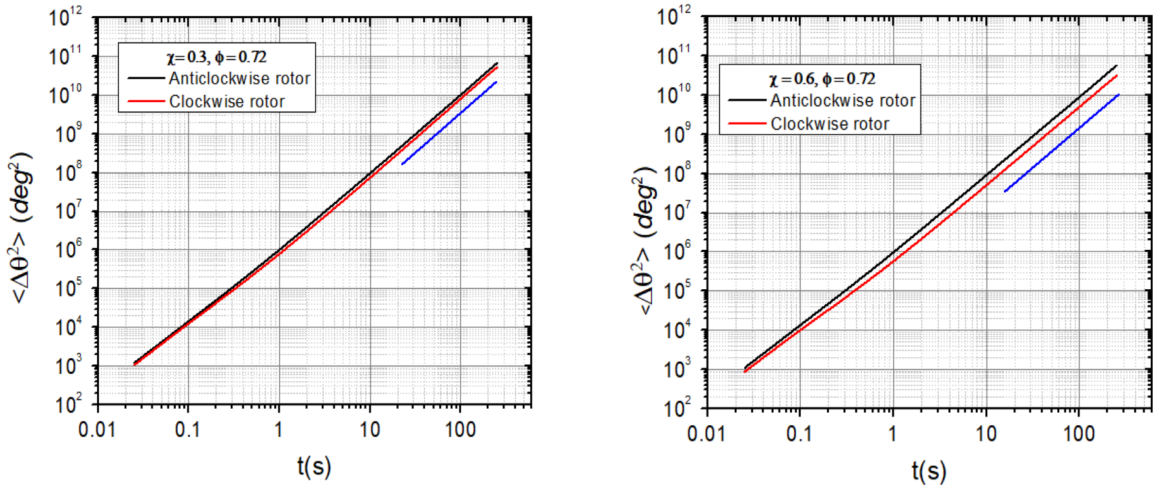

(a) (b)

Figure 3.6: Rotational MSD for clockwise and anticlockwise rotors. (a) Rotational MSD at $\phi = 0.72$ and $\chi = 0.3$, (b) MSD at $\phi = 0.72$ and $\chi = 0.6$.

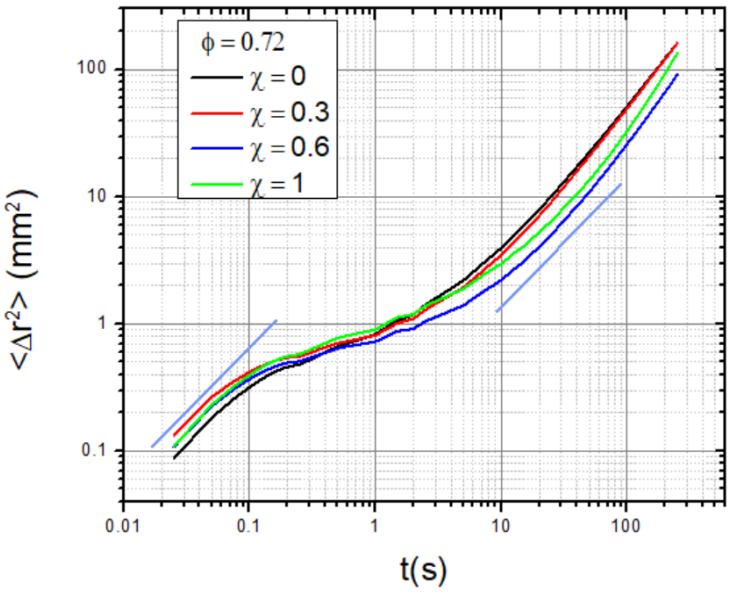

Figure 3.7: Mean square displacement (MSD) for different χ values at a fixed $\phi = 0.72$.

To probe the translational dynamics of active rotors, we plot mean square displacement

(MSD) for different χ values at a fixed $\phi = 0.72$ (see Fig. 3.7). For t $<$ 0.1s and t $>$ 10s the slope of these curves has a value of ≈ 1, indicating that these chiral particles are translationally diffusive in these regimes. No signs of re-entrant were observed for the translational degrees of freedom.

3.1.2 Non-Gaussian Parameter

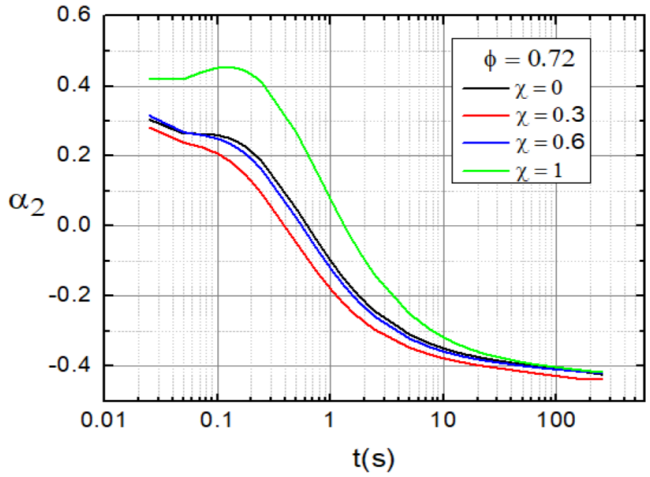

Figure 3.8: Rotational α_2 for the only clockwise rotors in a mixture of clockwise and anticlockwise rotors for different χ values at a fixed ϕ= 0.72.

The emergence of dynamical heterogeneities in a system with regions of less or more mobile particles than the average dynamics is a crucial feature of dense particle assemblies. The presence of these heterogeneities indicates that the structural relaxation in dense particle assemblies does not occur uniformly in the system. Dynamical heterogeneities can be quantified using the non-Gaussian parameter α_2, which calculates the deviation from Gaussian dynamics. Here,

$$\alpha_2 = \frac{\langle r^4(t)\rangle}{2\langle r^2(t)\rangle^2} - 1$$

and α_2(t) shows a maximum for supercooled liquids. For translational motion, at longer times, α_2 increases as the particles are momentarily trapped by their nearest neighbors. α_2 has a maximum at $t = t^*$, which corresponds to the cage breaking time. α_2 decreases

at a much longer time than t^* because particles go through multiple cage rearrangements.

To look for dynamical heterogeneities in the dense assemblies of active rotors, we plot angular α_2 as a function of time for $\phi = 0.72$ (see figure 3.8)

The peak values of angular α_2 show re-entrant with χ and are higher and shifted toward longer t^* for χ values of 0 and 1, indicating higher dynamic heterogeneity for $\chi =$ 0 and 1.

3.1.3 Cooperatively rearranging regions

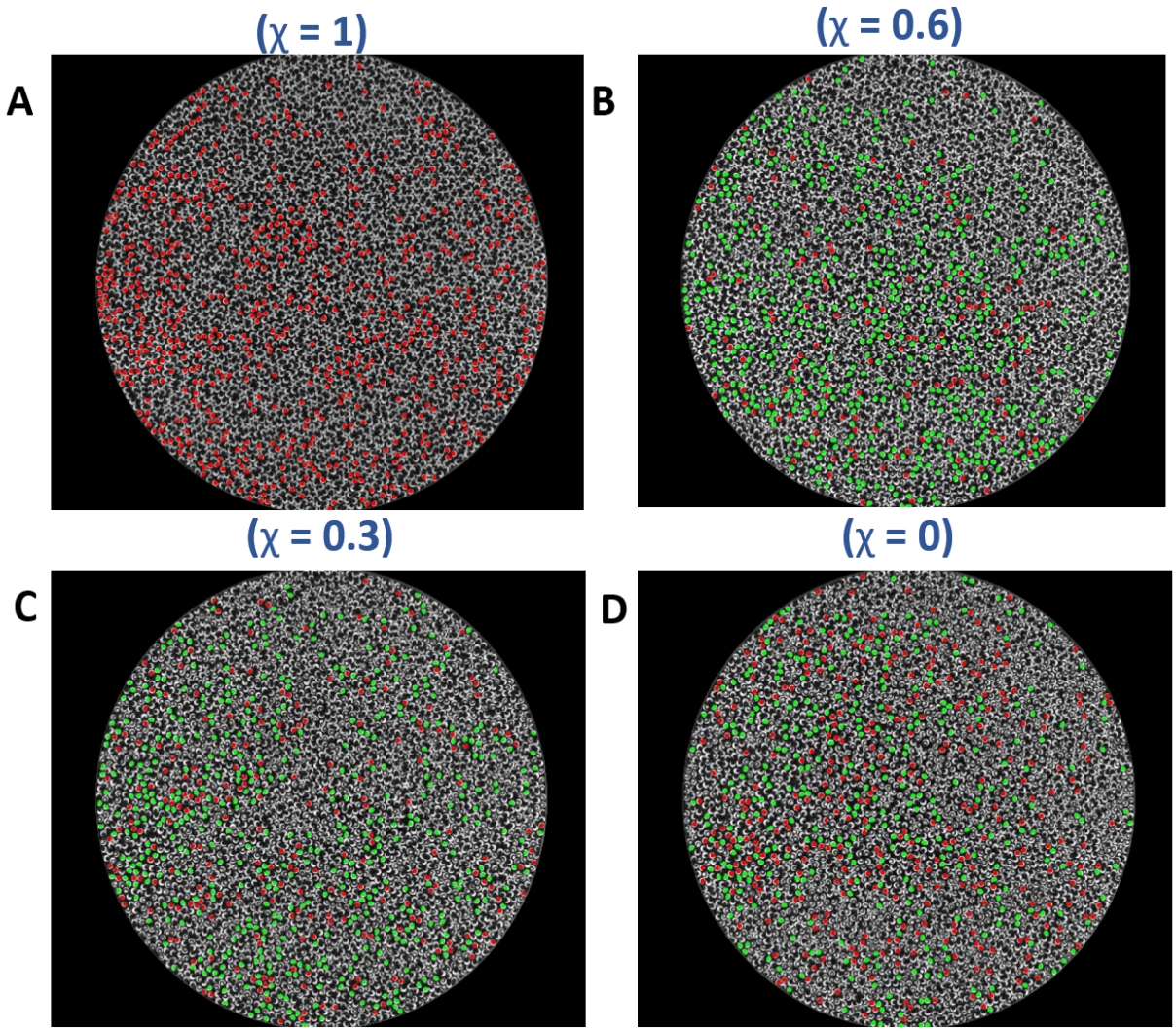

Figure 3.9: Rotational α_2 for the clockwise rotors at $\phi = 0.72$.

To check for signatures of cooperative particle dynamics, as found in glasses, we identify the top 20% most-mobile particles for different χ values at a fixed ϕ= 0.72 (see Fig 3.9). These most mobile particles, colored red(clockwise rotors) and green(anticlockwise rotors), were seen to be spatially clustered, and this was most evident in χ values of 0 and 1. This analysis however needs to be further refined to determine if the cluster size distribution shows a chirality dependence.

3.2 Observation of small and large angle grain boundaries at high ϕ

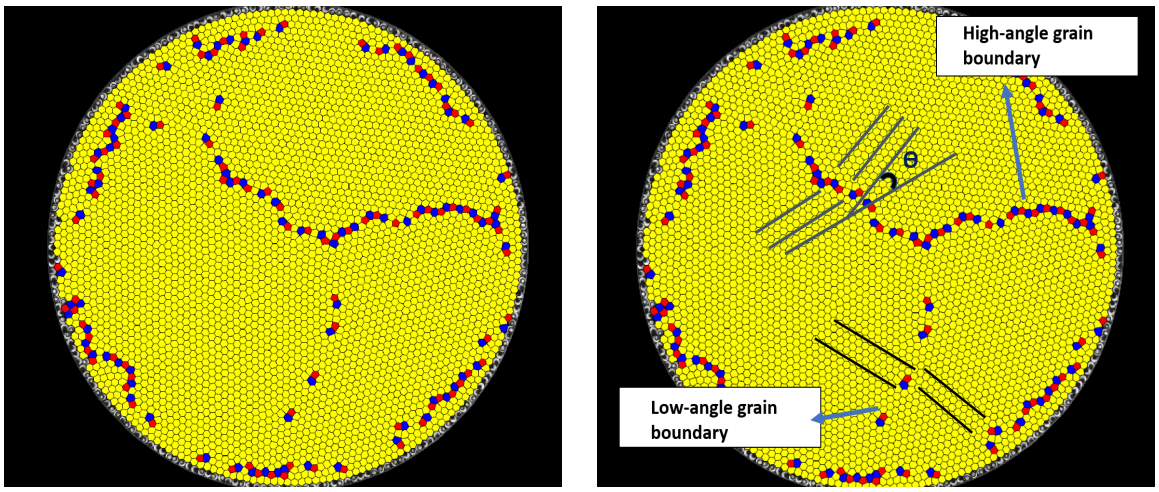

(a) (b)

Figure 3.10: Grain boundaries in the crystal formed by chiral active particles from the experiment. (a) 5-7 pairs at $\chi = 0$ and $\phi = 0.79$, (b) relative orientation of grains in figure a.

When ϕ was increased, the system of active rotors formed a polycrystal with well-defined grain boundaries between adjacent crystallites of differing orientation. These grain boundaries appeared as a series of dislocations (5-7 pairs) (see Fig. 3.10). The number of dislocations per unit length depended on the orientation mismatch between the adjacent crystallites. Small-angle grain boundaries were characterized by well-separated pairs while

for the large-angle grain boundaries the number density of 5-7 pairs was larger and they were also closely packed.

In the early 1950's Read and Shockley [12] studied a few simple grain boundaries in crystals based on the model for dislocations due to Burgers and Bragg. By counting the number of dislocations per unit length of the grain boundary, Read and Shockley provided a relationship between the energy of the grain boundary and the relative orientation of two grains ζ, the plot for which is shown in figure 3.11(a). The curve for Read and Shockley model saturates around the ζ values of 12 to 15.

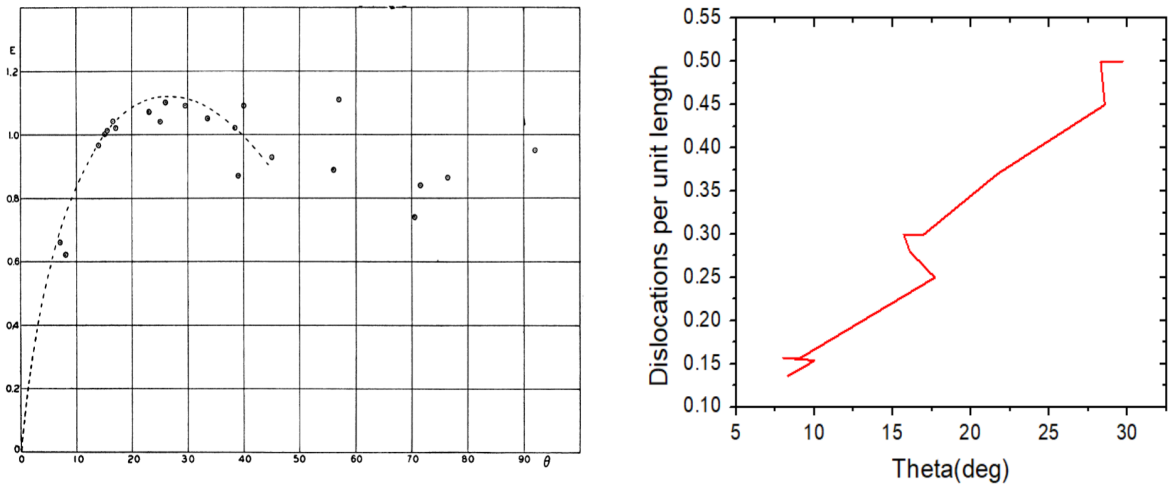

(a) (b)

Figure 3.11: Number of defect per unit length of a grain boundary as function of relative orientation of two grains (a) values from Read and Shokckley model, Adopted from [12] , (b) Values from our experiment with different ϕ values and at $\chi = 0$

A natural step for us was to determine if the Read and Shockley model developed for passive crystals also applies to crystals of active spinners. By counting the number of dislocations/defects per unit length at different values of times in the experiment for a fixed chirality, we plot the number of defects per unit length against the relative orientation of grains (see figure 3.11(b)). Since the rotors are circular in shape, the crystal formed by them is hexagonal, and thus the maximum relative orientation of grains can not exceed the ζ value of 30°. Interestingly, the curve, in contrast to the above-discussed model,

shows no sign of saturation, indicating that grain boundary energy and grain orientation relationship is very different in the case of chiral active crystals.

3.3 Conclusions and future perspectives

To conclude, our experiment shows a novel re-entrant in the total number of defects and angular MSD as a function of net chirality. Also, in contrast to the Read and Shockley models, our experiment shows that the number of dislocations per unit length of grain boundary does not saturate with the increasing relative orientation of two grains. We present the first experimental system where net chirality is varied systematically to study different properties in a system comprised of dense assemblies of chiral active rotors.

Since we can precisely tune the net chirality of the system in our experiment and can accommodate a vast number of particles on the plate, our experiments provide a well-controlled model system to study different interactions based on chirality, structural properties of chiral fluids and crystals, dynamics of dense assemblies of active rotors, and other different emergent properties in the case of chiral active matter systems.

The observation of re-entrants in the system of active rotors opens the door for many other fundamental questions about these systems. This includes the nature of interactions at the particle level; what is the nature of collision between two particles with the same and different chirality? How does the chirality of individual neighbors affect the dynamics of a given particle? Why does the system with a higher angular velocity contain less number of defects? Answers to these questions could uncover many new physics and thus help better understand these systems, which remains the future goal of this work.

Bibliography

[1] C. Dombrowski, L. Cisneros, S. Chatkaew, R. E. Goldstein, and J. O. Kessler, "Self-concentration and large-scale coherence in bacterial dynamics," *Phys. Rev. Lett.*, vol. 93, p. 098103, Aug 2004.

[2] N. Kumar, H. Soni, S. Ramaswamy, and A. K. Sood, "Flocking at a distance in active granular matter," *Nature Communications*, vol. 5, p. 4688, Sep 2014.

[3] J. Deseigne, O. Dauchot, and H. Chaté, "Collective motion of vibrated polar disks," *Phys. Rev. Lett.*, vol. 105, p. 098001, Aug 2010.

[4] C. Bechinger, R. Di Leonardo, H. Löwen, C. Reichhardt, G. Volpe, and G. Volpe, "Active particles in complex and crowded environments," *Rev. Mod. Phys.*, vol. 88, p. 045006, Nov 2016.

[5] M. C. Marchetti, J. F. Joanny, S. Ramaswamy, T. B. Liverpool, J. Prost, M. Rao, and R. A. Simha, "Hydrodynamics of soft active matter," *Rev. Mod. Phys.*, vol. 85, pp. 1143–1189, Jul 2013.

[6] D. Banerjee, A. Souslov, A. G. Abanov, and V. Vitelli, "Odd viscosity in chiral active fluids," *Nature Communications*, vol. 8, p. 1573, Nov 2017.

[7] X. Yang, C. Ren, K. Cheng, and H. P. Zhang, "Robust boundary flow in chiral active fluid," *Phys. Rev. E*, vol. 101, p. 022603, Feb 2020.

[8] P. Liu, H. Zhu, Y. Zeng, G. Du, L. Ning, D. Wang, K. Chen, Y. Lu, N. Zheng, F. Ye, and M. Yang, "Oscillating collective motion of active rotors in confinement," *Proceedings of the National Academy of Sciences*, vol. 117, no. 22, pp. 11901–11907, 2020.

[9] P. Arora, A. K. Sood, and R. Ganapathy, "Emergent stereoselective interactions

and self-recognition in polar chiral active ellipsoids," *Science Advances*, vol. 7, no. 9, p. eabd0331, 2021.

[10] D. M. Harris and J. W. Bush, "Generating uniaxial vibration with an electrodynamic shaker and external air bearing," *Journal of Sound and Vibration*, vol. 334, pp. 255–269, 2015.

[11] S. Ramaswamy, "The mechanics and statistics of active matter," *Annual Review of Condensed Matter Physics*, vol. 1, no. 1, pp. 323–345, 2010.

[12] W. T. Read and W. Shockley, "Dislocation models of crystal grain boundaries," *Phys. Rev.*, vol. 78, pp. 275–289, May 1950.

[13] V. Soni, E. S. Bililign, S. Magkiriadou, S. Sacanna, D. Bartolo, M. J. Shelley, and W. T. M. Irvine, "The odd free surface flows of a colloidal chiral fluid," *Nature Physics*, vol. 15, pp. 1188–1194, Nov 2019.

[14] B. A. Grzybowski and G. M. Whitesides, "Dynamic aggregation of chiral spinners," *Science*, vol. 296, pp. 718–721, 4/26/02 (no repr 2002. 792.

[15] C. Hargus, J. M. Epstein, and K. K. Mandadapu, "Odd diffusivity of chiral random motion," *Phys. Rev. Lett.*, vol. 127, p. 178001, Oct 2021.

[16] D. Geyer, D. Martin, J. Tailleur, and D. Bartolo, "Freezing a flock: Motility-induced phase separation in polar active liquids," *Phys. Rev. X*, vol. 9, p. 031043, Sep 2019.

[17] S. Dey, D. Das, and R. Rajesh, "Spatial structures and giant number fluctuations in models of active matter," *Phys. Rev. Lett.*, vol. 108, p. 238001, Jun 2012.

[18] Y. Hatwalne, S. Ramaswamy, M. Rao, and R. A. Simha, "Rheology of active-particle suspensions," *Phys. Rev. Lett.*, vol. 92, p. 118101, Mar 2004.

[19] T. B. Liverpool and M. C. Marchetti, "Rheology of active filament solutions," *Phys. Rev. Lett.*, vol. 97, p. 268101, Dec 2006.

[20] J. R. Howse, R. A. L. Jones, A. J. Ryan, T. Gough, R. Vafabakhsh, and R. Golestanian, "Self-motile colloidal particles: From directed propulsion to random walk," *Phys. Rev. Lett.*, vol. 99, p. 048102, Jul 2007.

[21] C. W. Reynolds, "Flocks, herds and schools: A distributed behavioral model," *SIGGRAPH Comput. Graph.*, vol. 21, p. 25–34, aug 1987.

[22] T. Vicsek, A. Czirók, E. Ben-Jacob, I. Cohen, and O. Shochet, "Novel type of phase transition in a system of self-driven particles," *Phys. Rev. Lett.*, vol. 75, pp. 1226–1229, Aug 1995.

[23] G. E. Uhlenbeck and L. S. Ornstein, "On the theory of the brownian motion," *Phys. Rev.*, vol. 36, pp. 823–841, Sep 1930.

[24] T. Sanchez, D. T. N. Chen, S. J. DeCamp, M. Heymann, and Z. Dogic, "Spontaneous motion in hierarchically assembled active matter," *Nature*, vol. 491, pp. 431–434, Nov 2012.

[25] V. Narayan, S. Ramaswamy, and N. Menon, "Long-lived giant number fluctuations in a swarming granular nematic," *Science*, vol. 317, no. 5834, pp. 105–108, 2007.